

SIMULATIONS OF GALAXY FORMATION IN A Λ CDM UNIVERSE III: THE DISSIPATIVE FORMATION OF AN ELLIPTICAL GALAXY

ANDRÉS MEZA AND JULIO F. NAVARRO¹

Department of Physics and Astronomy, University of Victoria, Victoria, BC V8P 1A1, Canada

MATTHIAS STEINMETZ²

Steward Observatory, 933 North Cherry Avenue, Tucson, AZ 85721, USA, and Astrophysikalisches Institut Potsdam, An der Sternwarte 16, D-14482 Potsdam, Germany

AND

VINCENT R. EKE³

Physics Department, Durham University, South Road, Durham DH1 3LE, England

The Astrophysical Journal, 590:619-635, 2003 June 20

ABSTRACT

We examine the dynamical structure of an elliptical galaxy simulated in the Λ CDM scenario. The morphology of the galaxy evolves dramatically over time in response to the mode and timing of mass accretion; smooth deposition of cooled gas leads to the formation of centrifugally supported disks, whilst major mergers disperse stellar disks into spheroids. In the case we consider here, these two modes of accretion alternate successively until $z \sim 0.6$, when the galaxy undergoes one last major (1:3) merger. The event triggers a starburst that consumes much of the remaining gas into stars. Little gas cools and accretes subsequently and, as a result, most stars at $z = 0$ are rather old (75% are older than 9 Gyr), and distributed in a spheroidal component that resembles present-day elliptical galaxies. Dynamically, the galaxy is well approximated by an E4 oblate rotator, with rotational support increasing steadily from the center outwards. The apparent rotation support, as measured by V_{rot}/σ , correlates strongly with isophotal deviations from perfect ellipses. Boxy isophotes are obtained when the galaxy is seen face-on and $V_{\text{rot}}/\sigma \ll 1$. On the other hand, disky isophotes are found for inclinations which maximize V_{rot}/σ . The line-of-sight velocity distribution is nearly Gaussian at all radii, although small but significant deviations are robustly measured. The sign of the Gauss-Hermite skewness parameter h_3 is anti-correlated with the apparent sense of rotation, in agreement with observed trends. Despite its relatively recent assembly, the simulated galaxy has much higher effective surface brightness than normal ellipticals of similar luminosity, in a way reminiscent of the less common type of M32-like “compact ellipticals”. This is likely a direct consequence of our star formation and feedback algorithm, which allows for efficient transformation of gas into stars in dense, early collapsing progenitors rather than a definitive prediction for the structure of galaxies assembled in this Λ CDM halo. Despite this limitation, our simulation suggests that dark matter plays a minor role in the luminous regions of compact ellipticals, whose dynamical mass-to-light ratios are thus not dissimilar to those of normal ellipticals. This explains the proximity of compact ellipticals to edge-on projections of the Fundamental Plane, despite their far greater velocity dispersion at given luminosity. Overall, our simulation shows that repeated episodes of dissipational collapse, followed by merger events, lead to stellar spheroids that are only mildly triaxial and of relatively simple kinematic structure. This is in better agreement with observation than earlier models based on dissipationless mergers of stellar disks, and a positive step towards reconciling the observed structure of ellipticals with a hierarchical assembly process where mergers play a substantial role.

Subject headings: galaxies: elliptical and lenticular, cD — galaxies: formation — galaxies: interactions — methods: N-body simulations

1. INTRODUCTION

Elliptical galaxies constitute a rather uniform family of stellar spheroids whose dynamical and photometric properties satisfy a number of scaling relations and whose detailed internal structure appear to vary weakly but systematically with galaxy mass. Perhaps the most important of such scaling relations is the Fundamental Plane; a tight correlation between the luminosity, size, and velocity dispersion that has been extensively used as a sensitive distance indicator (Djorgovski & Davis 1987; Dressler et al. 1987). The existence of the Funda-

mental Plane is believed to reflect largely the virial theorem, as applied to systems where the dark matter content, as well as perhaps age and metallicity, vary monotonically as a function of luminosity.

Subtler dynamical and photometric indicators also vary with luminosity; bright ellipticals are typically slowly-rotating triaxial structures supported by anisotropic velocity dispersion tensors, whereas rotation is thought to play a more substantial role in the dynamics of fainter ellipticals (Davies et al. 1983; Bender & Nieto 1990; Halliday et al. 2001). This dynamical distinction is reflected in isophotal deviations from perfect ellipses: fast-rotating spheroids are usually “disky”, in contrast with the “boxy” isophotal shapes of slowly rotating systems (Bender 1988). Such deviations—although signifi-

¹ Fellow of the Canadian Institute for Advanced Research and of the Alfred P. Sloan Foundation

² Packard Fellow and Sloan Fellow

³ Royal Society University Research Fellow

cant and robustly measured—are usually small, and simple concentric ellipsoidal models provide a rough but reasonable description of the structure of many elliptical galaxies. Indeed, detailed dynamical analysis indicates that most ellipticals are globally only mildly triaxial, as indicated, for example, by the weak misalignment between photometric and dynamical principal axes (de Zeeuw & Franx 1991; Franx, Illingworth, & de Zeeuw 1991).

These structural trends hold important clues to the formation and evolution of ellipticals, and are not straightforward to account for in traditional models of elliptical galaxy formation. In the “monolithic collapse” model put forward by Partridge & Peebles (1967), all stars in an elliptical galaxy form coevally at very early times as a result of the coherent, dissipationless collapse of a large mass of gas transformed into stars in a short and intense bout of star formation. This simple model accounts naturally for the old apparent ages of spheroid stars, for their high densities, and for the weak evolution in the spheroidal population properties with time, but is less successful at explaining the detailed luminosity dependence of their dynamical properties; the apparent scarcity of very large starbursts in the high-redshift universe; and the origin of dynamical peculiarities suggestive of recent accretion events (e.g., Franx & Illingworth 1988; Jedrzejewski & Schechter 1988; Surma & Bender 1995; de Zeeuw et al. 2002).

In its most extreme form, the competing “hierarchical assembly” model posits that spheroidal galaxies form through the violent merger of preexisting disk galaxies (Toomre 1977). In this scenario, the epoch of assembly of ellipticals differs markedly from the epoch of formation of their constituent stars, and the high density of ellipticals is ascribed to the effects of dissipation during the formation of the progenitor disks. This model accounts “naturally” for the scarcity of very bright elliptical progenitors at high-redshift; for the rapid evolution of the galaxy population with lookback time; and for the presence of dynamical peculiarities. It is, on the other hand, less successful at explaining the apparent old ages of stars in ellipticals and the uniformity in their dynamical properties. Indeed, it has been plausibly argued that the remnants of major mergers between stellar disks cannot reproduce the steep central surface brightness profiles of ellipticals, and that dissipationless merger remnants are too triaxial, anisotropic, and kinematically peculiar to be consistent with normal ellipticals (Barnes 1992; Hernquist 1992, 1993).

One possible solution to these problems is to argue that the hierarchical mergers that lead to the formation of ellipticals are gas-rich, and that substantial dissipation takes place during the collision, where renewed star formation of gas driven to the center can steepen the luminosity profiles and even out misalignments in the dynamical structure. This possibility has been explored by Mihos & Hernquist (1994; and references therein) who find that major mergers may actually be too efficient at funneling gas towards the center, leading to extremely dense stellar cores in disagreement with observation.

Taken together, this body of work suggests that it might indeed be possible to reconcile the observed structural properties of ellipticals with the hierarchical formation scenario, but only provided that star formation somehow regulates effectively the flow of accreting gas within galaxies, especially during mergers. Thus, accounting self-consistently for the frequency of merging—which is determined largely by the cosmological context of formation—is crucial for the success of the modeling and has yet to be taken into account properly in simulation work.

We present here the result of our first attempt at simulating the formation of an elliptical galaxy *ab initio* within the popular Λ CDM cosmogony. The simulation evolves self-consistently a region destined to aggregate into a single dark matter halo and includes the gravitational and hydrodynamical effects of dark matter and baryons, photo-heating by a UV background, Compton and radiative cooling, as well as star formation and feedback processes. The main evolutionary features of this simulation have been presented by Steinmetz & Navarro (2002). This is one of the new generation of simulations able to resolve the internal dynamics of galaxies whilst accounting properly for the cosmological context of the formation process (see also Abadi et al. 2003a,b; Governato et al. 2002; Sommer-Larsen et al. 2002a,b). In this paper, we focus on the $z = 0$ structure and kinematics of the stellar component of the simulation reported by Steinmetz & Navarro (2002).

Major aims of this paper are to validate the analysis techniques that we intend to apply to a statistically meaningful set of simulations (under preparation) of comparable numerical resolution, as well as to identify potential disagreements between simulation and observation that may prompt a radical revision of our simulation algorithm or of the adopted cosmological model. The plan of this paper is as follows. Section 2 presents a brief description of our numerical techniques, whereas § 3 presents the main results of the simulation. We summarize our findings in § 4.

2. NUMERICAL METHODS

2.1. *The Code*

The simulation was performed using GRAPESPH, a code that combines the hardware N-body integrator GRAPE with the smoothed-particle hydrodynamics (SPH) technique (Steinmetz 1996). GRAPESPH is a fully three-dimensional, Lagrangian technique optimally suited to study the formation of highly nonlinear systems in a cosmological context. The version used here includes the self-gravity of gas, stars, and dark matter; a three-dimensional treatment of the hydrodynamics of the gas; Compton and radiative cooling; the effects of a photoionizing UV background (Navarro & Steinmetz 1997); as well as a simple recipe for transforming gas into stars.

The numerical recipe for star formation, feedback and metal enrichment is similar to that described in Steinmetz & Müller (1994, 1995; see also Katz 1992; Navarro & White 1993). In this scheme, star particles are created in collapsing regions that are locally Jeans unstable, at a rate controlled by the local cooling and dynamical timescales, $\dot{\rho}_* = c_* \rho_{\text{gas}} / \max(\tau_{\text{cool}}, \tau_{\text{dyn}})$. The parameter c_* effectively controls the depletion timescale of gas in regions of high density, where most star formation takes place and where $\tau_{\text{dyn}} \gg \tau_{\text{cool}}$. Star particles are only affected by gravitational forces, but they devolve $\sim 10^{49}$ ergs (per solar mass of stars formed) into their surrounding gas over the $\sim 3 \times 10^7$ yrs following their formation. This energy input—a crude attempt to mimic the energetic feedback from evolving massive stars and supernovae—is mainly invested into raising the internal energy (temperature) of the surrounding gas. However, because stars form in high-density regions, where cooling timescales are short, this feedback energy is almost immediately radiated away.

In order to allow for more effective feedback we assume that a certain fraction of the available energy, ϵ_v , is invested in modifying the kinetic energy of the surrounding gas. These

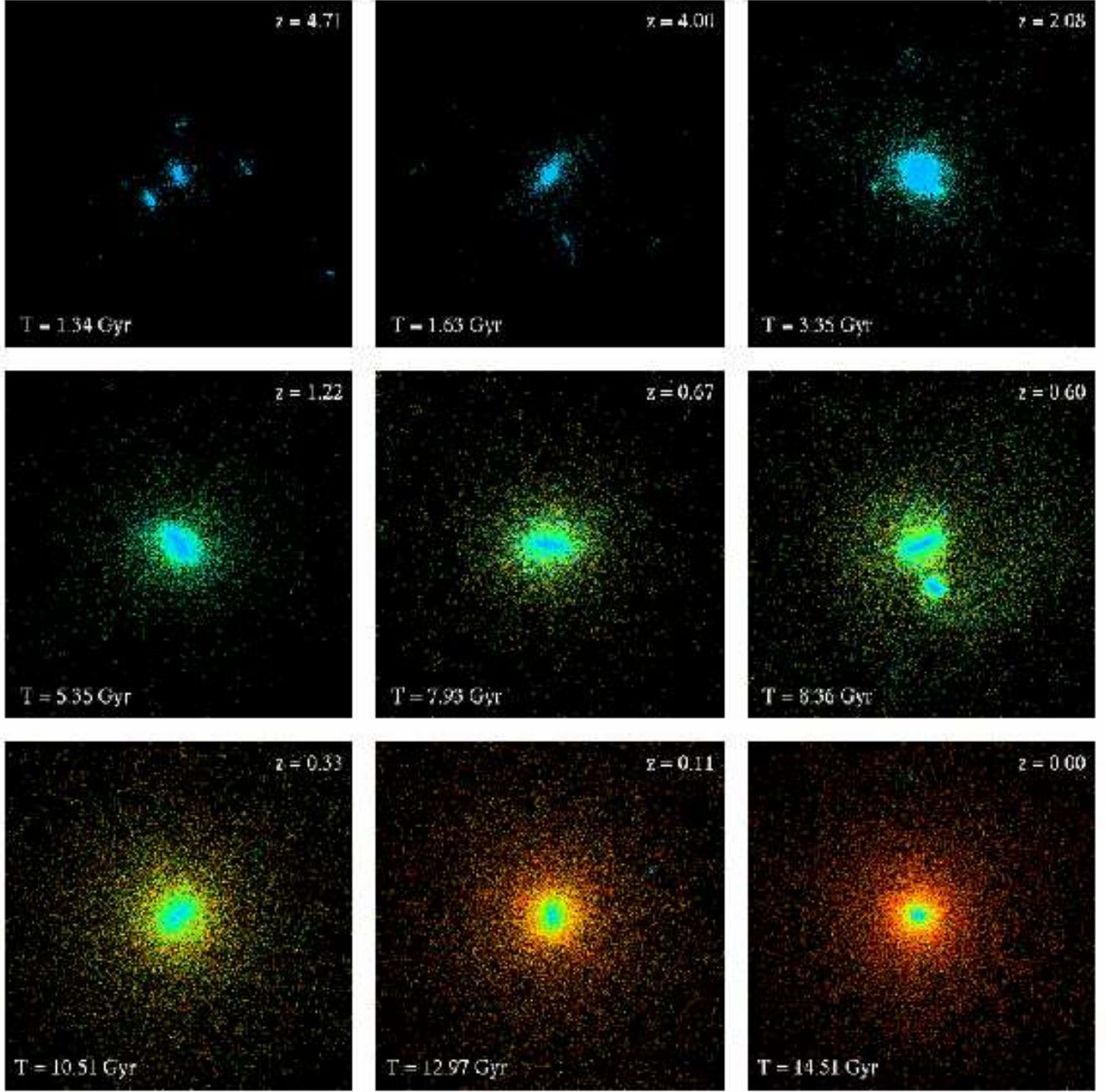


FIG. 1.— Star particles within a cube of 40 physical kpc on a side, shown at different redshifts and projected so that the luminous component of the galaxy at $z = 0$ is seen approximately face-on. Each particle is colored according to its age at the time shown. Blue and red correspond to $\tau \lesssim 4$ Gyr and $\tau \gtrsim 10$ Gyr, respectively. Note that the plotting routine overlays young particles over old and thus somewhat overemphasizes the importance of young stellar components.

gas motions can still be dissipated through shocks, but on longer timescales, reducing the star formation efficiency and extending the timescale for the conversion of gas into stars. Our star formation recipe thus involves two free parameters, c_* and ϵ_v , which we set by matching the star formation rate of isolated disks to those observed in the local universe (Kenricutt 1998). We have adopted $c_* = 0.033$ and $\epsilon_v = 0.05$ in the simulation reported here. This is a conservative choice in the sense that the resulting feedback is relatively inefficient at regulating star formation: the rate at which gas cools and accretes at the center of dark matter halos effectively determines the star formation rate.

2.2. Initial Conditions

The simulation assumes the popular “concordance” Λ CDM scenario; a flat, low-density universe ($\Omega_0 = 0.3$, $\Omega_\Lambda = 0.7$) where the mass is dominated by Cold Dark Matter, with a modest baryonic contribution ($\Omega_b = 0.019 h^{-2}$). The present day expansion rate is parameterized by $h = H_0/(100 \text{ km s}^{-1} \text{ Mpc}^{-1}) = 0.65$. The Λ CDM power spectrum is normalized so that the linear present-day rms mass fluctuations on spheres of radius $8 h^{-1} \text{ Mpc}$ is $\sigma_8 = 0.9$.

We simulate a region that evolves to form at $z = 0$ a dark halo of mass $\sim 3 \times 10^{12} M_\odot$. This halo is selected from

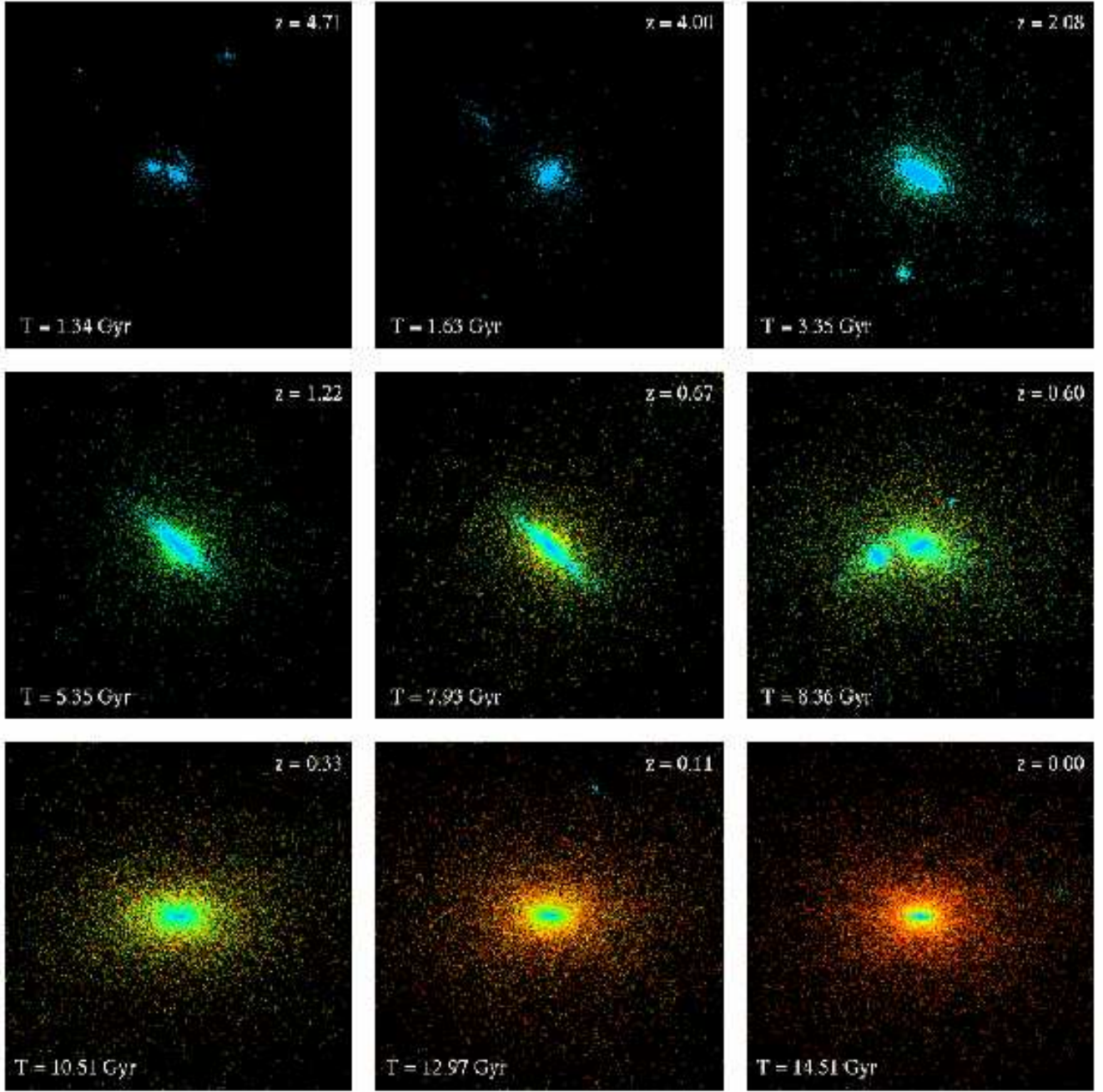


FIG. 2.— As in Figure 1, but rotated 90 degrees so that the galaxy at $z = 0$ is seen approximately edge-on.

a cosmological simulation of a periodic $32.5 h^{-1}$ Mpc box and resimulated at higher resolution, including the full tidal field of the original calculation. Details on this procedure may be found in Katz & White (1993), Navarro & White (1994) and Navarro & Steinmetz (1997, 2000). The mass of gas and dark matter particles is initially $1.28 \times 10^7 M_\odot$ and $7.24 \times 10^7 M_\odot$, respectively. The (Plummer) gravitational softening lengthscale is fixed at 0.5 (physical) kpc.

2.3. Analysis

Galaxy luminosities are computed by simply adding the luminosities of each star particle, taking into account the time of creation of each particle and using the latest version of the

spectrophotometric models of Contardo, Steinmetz, & Fritz-von Alvensleben (1998). We assume that the stellar Initial Mass Function (IMF) is independent of time. Quantitative measures quoted in this paper assume a Scalo (1986) IMF truncated at 0.1 and $100 M_\odot$, respectively, unless explicitly stated otherwise. The spectrophotometric modeling requires a measure of the metallicity of the stars. GRAPESPH tracks (crudely) the metal content of each gaseous particle by assuming that each “star” devolves a total of $1.7 M_\odot$ of enriched material (per $100 M_\odot$ of stars formed) to the surrounding gas during the 3×10^7 yrs following its creation. These metals are dispersed amongst the gas particles neighboring the star, and their metal content is in turn inherited by the star particles

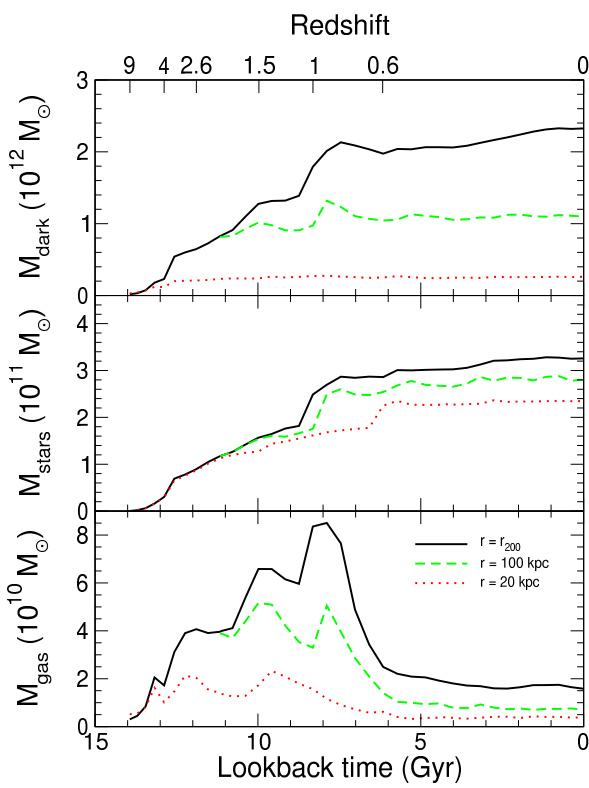


FIG. 3.— The mass evolution of the dark matter, stellar and gas components of the simulated galaxy, measured within different spherical shells centered on the main luminous progenitor. Solid lines correspond to the mass within the virial radius, r_{200} , dashed lines to the mass within 100 (physical) kpc, and dotted lines to the mass within the luminous radius, $r_{\text{lum}} = 20$ (physical) kpc.

they spawn. Our treatment of metal enrichment neglects diffusion processes and is not intended to reproduce the Fe-rich enrichment by type Ia supernovae, which is thought to occur on a much longer timescale. Given its crudeness, we restrict our use of the metallicity of gas and stars to the spectrophotometric modeling of the stellar populations. It is our intention, however, to include in future work a self-consistent treatment of metal enrichment by type I and II supernovae in order to tap the potential of heavy element abundance patterns in judging the success of the modeling. This is an important task, as it has been argued that it might be difficult to reproduce the alpha element-enhanced abundance of ellipticals in hierarchical scenarios of formation (see, e.g., Thomas 2001 and references therein).

3. RESULTS

3.1. The Assembly of an Elliptical Galaxy

As described in detail by Steinmetz & Navarro (2002), the formation of the galaxy is characterized by episodes of smooth accretion and by a number of merger events, some of which are clearly visible in Figures 1 and 2. These figures show the stellar component within a 40 (physical) kpc box centered on the most massive progenitor at different times. Star particles are colored according to age (blue and red correspond to ages $\lesssim 4$ and $\gtrsim 10$ Gyr, respectively). Figure 1 (2) shows the system projected along an axis chosen so that the galaxy at $z \sim 0$ is seen face-on (edge-on).

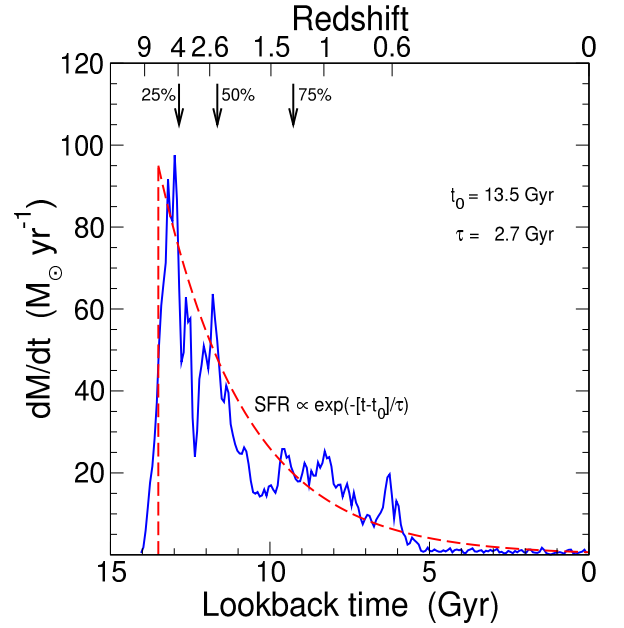


FIG. 4.— Age distribution of all stars within the luminous radius at $z = 0$. Downward-pointing arrows indicate the time of formation of the first 25%, 50%, and 75% of the stars, respectively. Major mergers are typically associated with short bursts of star formation that show as peaks in the age distribution. Overall, the age distribution is well approximated by an exponential law of age $t_0 = 13.5$ Gyr and e-folding timescale $\tau = 2.7$ Gyr (see dashed line). This is comparable to what is usually assumed in spectrophotometric modeling of the spectral energy distribution of elliptical galaxies (Guiderdoni & Rocca-Volmerange 1987; Bruzual & Charlot 1993).

The morphology of the galaxy varies substantially in response to changes in the dominant mode of mass accretion. Mergers between progenitors of comparable mass are frequent at early times. One of these events is clearly visible in the top left panels of Figures 1 and 2. Major mergers mix stars into a spheroid, around which smoothly accreting gas may subsequently wrap to form a new disk-like component. At $z \sim 2$ the simulated galaxy resembles a bright Sa/Sb spiral: over 70% of the rest-frame optical luminosity comes from a roughly exponential disk while the rest comes from a spheroidal component whose spatial distribution may be well approximated by an $R^{1/4}$ -law.

The disk continues to grow gradually until it is tidally shaken by a massive satellite (seen in the $z = 2.08$ panel of Figures 1 and 2) into a clearly-defined barred pattern. The bar is resilient and survives the accretion (at $z = 1.6$) of the satellite that triggered its formation. At $z \sim 0.6$, the galaxy undergoes a further and final major merger with another disk galaxy about one third as massive. During the collision, the remaining gas ($\lesssim 8\%$ of the total baryonic mass) is efficiently funneled to the center, where it is quickly converted into stars (Barnes & Hernquist 1991). This last episode of star formation is effectively over by $z = 0.5$, leaving only a small (~ 1 kpc diameter) ‘core’ of younger, metal-rich stars, surrounded by a large spheroid of older stars. Morphologically, the $z \sim 0.6$ merger turns the galaxy from a centrifugally supported disk into a slowly-tumbling spheroid that quickly relaxes into the final configuration which is the subject of the study we report here.

Quantitatively, the mass assembly process is summarized in Figure 3, where we plot the evolution of the mass in the dark

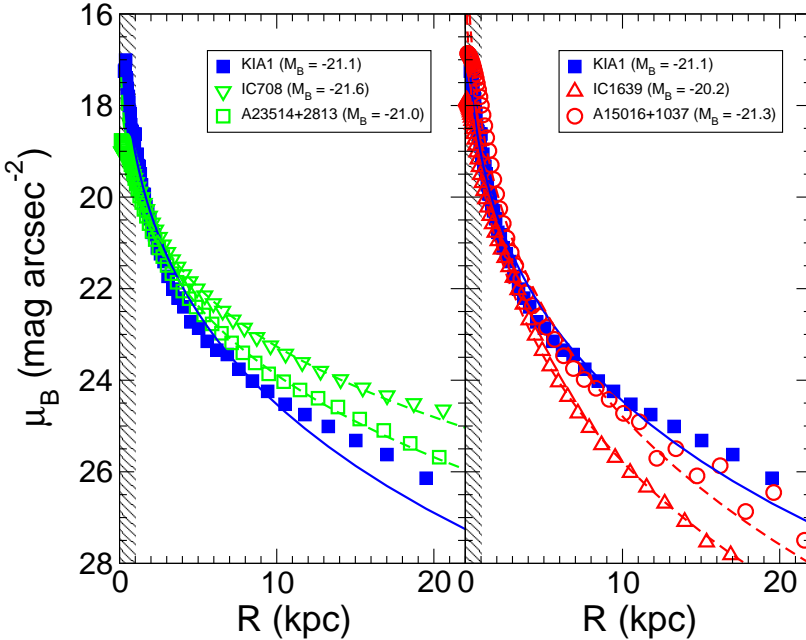


FIG. 5.— B-band surface brightness profile of the simulated galaxy (labeled KIA1) as a function of projected radius R . The left panel compares it with two “normal” elliptical galaxies of similar luminosity from the Nearby Field Galaxy Survey of Jansen et al. (2000). The right-hand panel compares KIA1 with two “compact” ellipticals from the same survey. Clearly, the simulated galaxy is much more concentrated than normal ellipticals of comparable luminosity, and bears a closer resemblance to compact ellipticals. Lines through the symbols illustrate the best $R^{1/4}$ fit for each profile.

matter, gas, and stellar components within various radii. From top to bottom, the curves in Figure 3 correspond to the mass within the virial radius⁴, r_{200} ; within 100 (physical) kpc; and within the “luminous” radius, $r_{\text{lum}} = 20$ (physical) kpc. All of these curves show that the assembly of the galaxy is essentially complete by $z = 0.6$, just after the last major accretion event. Indeed, the mass within r_{lum} remains approximately constant after that time, although that within r_{200} continues to increase, mainly due to the time-dependent definition of the virial radius. The $z = 0.6$ merger leads to a short starburst that depletes (into stars) the last $\sim 4 \times 10^9 M_{\odot}$ of gas within the merging galaxies. The final stellar mass of the galaxy is essentially fixed at this event, since little gaseous material is added to the galaxy afterwards; stars age passively for the remaining ~ 7 Gyr of the evolution. The galaxy thus has no opportunity to re-form a stellar disk, and its morphology at $z = 0$ is consistent with that of elliptical galaxies. Some of the properties of the galaxy at $z = 0$ are summarized in Tables 1 and 2.

The evolutionary features discussed above are easily recognizable in the age distribution of stars (Figure 4). Most stars identified within r_{lum} at $z = 0$ are old; the first 25% of the stars form before $z \sim 4$; the median formation redshift is $z \sim 2.4$ and only 2% of the stars have formed in the past 5 Gyr. The dashed line in Figure 4 shows that, overall, the age distribution compares well with that expected from an exponentially declining star formation rate, $\dot{M}_* \propto e^{-t/2.7\text{Gyr}}$,

⁴ We define the virial radius as the radius where the mean inner density contrast (relative to the critical density for closure) is 200; i.e., $\bar{\rho}(r_{200}) = 200 \times 3 H^2(z)/8\pi G$. We parameterize the present value of Hubble’s constant as $H(z = 0) = H_0 = 100 h \text{ km s}^{-1} \text{ Mpc}^{-1}$. All distance-dependent quantities assume $h = 0.65$.

initiated 13.5 Gyrs ago. These parameters are not dissimilar from those used to model elliptical galaxies spectrophotometrically (e.g., Guiderdoni & Rocca-Volmerange 1987; Bruzual & Charlot 1993), so we expect the broad-band colors and other major photometric indicators of the simulated galaxy to be in reasonable agreement with those of elliptical galaxies. The numerical resolution achieved in this simulation (at $z = 0$ there are more than 65000 stars within the luminous radius, r_{lum}) allows us to examine in detail the structure of the simulated galaxy and to assess whether the morphological likeness to an elliptical at $z = 0$ is further substantiated by the detailed photometric and kinematic properties of the galaxy. We turn our attention to this issue next.

3.2. Photometric Properties

3.2.1. Surface brightness profile

The face-on surface brightness profile (computed using circularly symmetric apertures) of the simulated galaxy (labeled KIA1 for short) at $z = 0$ is shown in the left panel of Figure 5 (solid symbols) and compared with two elliptical galaxies of similar B -band absolute magnitude selected from the Nearby Field Galaxy Survey of Jansen et al. (2000). There are no rescalings allowed in this figure and therefore the mismatch between simulated and observed ellipticals is genuine: the simulated galaxy is significantly more concentrated than IC708 (open triangles) and A23514+2813 (open squares). This is confirmed by the effective radii of these galaxies: in the B -band the effective radius of KIA1 is $R_e = 1.3$ kpc, but those of IC708 and A23514+2813 are $R_e = 11.3$ and 5.8 kpc, respectively. The simulated galaxy thus resembles examples of the much rarer class of M32-like “compact” ellipticals, such as A15016+1037 or IC1639, shown in the right

TABLE 1. MAIN PROPERTIES OF SIMULATED GALAXY AT $z = 0$

Radius (kpc)	M_{tot} ($10^{11} M_{\odot}$)	M_{dm} ($10^{11} M_{\odot}$)	M_{stars} ($10^{11} M_{\odot}$)	M_{gas} ($10^{10} M_{\odot}$)	V_{circ} (km s $^{-1}$)
r_{200}	26.66	23.25	3.26	1.58	195.3
200	21.49	18.31	3.06	1.21	214.9
100	13.87	11.00	2.80	0.71	244.2
20	4.99	2.60	2.35	0.38	327.5
$2R_e$	2.05	0.54	1.51	0.11	578.2
R_e	1.45	0.36	1.08	0.06	687.8

NOTE. — All quantities are measured within the radii given in column [1] and assume $h = 0.65$. The virial radius at $z = 0$ is $r_{200} = 300.5$ kpc. The mass per particle is $m_{\text{dm}} = 7.24 \times 10^7 M_{\odot}$ for the dark matter. In total, there are 32090 dark matter particles within r_{200} . Initially (before any star formation takes place) the gas particle mass is $1.28 \times 10^7 M_{\odot}$. There are 87669 star particles within r_{200} , not all of the same mass; the average star particle mass is $3.72 \times 10^6 M_{\odot}$. The effective radius at $z = 0$ is $R_e = 1.32$ kpc, measured in the B -band.

TABLE 2. PHOTOMETRIC PROPERTIES OF SIMULATED GALAXY

Band	L_{tot} ($10^{10} L_{\odot}$)	M [mag]	R_e [kpc]	μ_0^{fit} [mag arcsec $^{-2}$]	R_e^{fit} [kpc]	$\langle \mu \rangle_e$ [mag arcsec $^{-2}$]
U	3.32	-20.7	1.34	12.2	1.78	18.5
B	4.16	-21.1	1.32	11.8	1.75	18.1
R	6.65	-22.6	1.29	10.2	1.72	16.5
K	19.80	-25.0	1.17	7.7	1.58	13.9

NOTE. — Luminosities and radii assume face-on projection, $h = 0.65$ and a Scalo IMF with an upper and lower mass cutoffs of 100 and $0.1 M_{\odot}$, respectively.

panel of Figure 5. These are galaxies of unusually small effective radii (or unusually high surface brightness) for their luminosity; the effective radii are $R_e = 1.2$ and 1.7 kpc for A15106+1037 and IC1639, respectively, comparable to that measured for KIA1.

The high concentration of the stellar component may be traced to the copious star formation that accompanies at high redshift the dissipative collapse of the galaxy’s progenitors. These progenitors are extremely dense and compact, and their density is inherited by the final remnant. It is not clear at this time whether this is a generic prediction of this cosmogony or of a simulation procedure where feedback affects only minimally the timing and mode of gas cooling and accretion. Indeed, results reported by other groups (Governato et al. 2002; Sommer-Larsen et al. 2002a,b), indicate that it is likely that a different implementation of star formation and feedback—e.g., one that prevents more effectively the onset of star formation in early collapsing progenitors—might bring simulations into better agreement between the observed structure of normal galaxies.

3.2.2. Colors

The numerous merger episodes that characterize the formation of the simulated galaxy lead to a fairly uniform stellar component with little sign of radial gradients in stellar age. This is reflected in the rather uniform color profiles shown in Figure 6. This figure compares the $B-R$ and $U-B$ color profiles of KIA1 with four ellipticals shown in Figure 5. Because of its old age, the colors of the simulated galaxy are quite red, comparable to those of normal ellipticals (top panel in Figure 6). On the other hand, the colors of compact ellipticals are typically bluer and show greater variety than those of normal ellipticals. Furthermore, observed ellipticals show a mild propensity for reddish cores which is not reproduced in the

simulated galaxy. It is likely, however, that such a tendency is a result of metallicity gradients, which would be poorly captured by our rudimentary numerical treatment of metal enrichment.

To summarize, the simulated elliptical is morphologically closer to a compact elliptical than to a normal one, but it appears as if its stellar population resembles more that of normal ellipticals. Thus, to bring the simulated galaxy into closer agreement with observation one would need to either distort the tightly bound stellar structure of the simulated galaxy without changing its colors or else allow for recent episodes of star formation in order to account for the bluer colors of compact ellipticals. Either alternative would require a major revision to the way in which star formation and feedback are modeled in our numerical code. This result is similar to that reported by Abadi et al. (2003a) for a simulated disk galaxy in the Λ CDM scenario. Since Abadi et al. used the same numerical code as in the present study, it appears as if stellar systems that are too concentrated to be consistent with observation are a generic feature of our simulation procedure. We intend to explore systematically the sensitivity of this result to our choice of star formation and feedback algorithm in future papers of this series.

3.2.3. Shape and rotation

Figure 7 contrasts the photometric structure of the simulated galaxy with a map of the line-of-sight mean velocity field along 10 different projections. Each panel corresponds to 10 kpc boxes projected so that the inclination of the galaxy increases successively by 10 degrees from top-left (face-on projection) to bottom-right (edge-on view). The orientation is chosen so that the projected major axis is aligned horizontally in all panels. By construction, the apparent ellipticity of the galaxy increases along the panel sequence, from

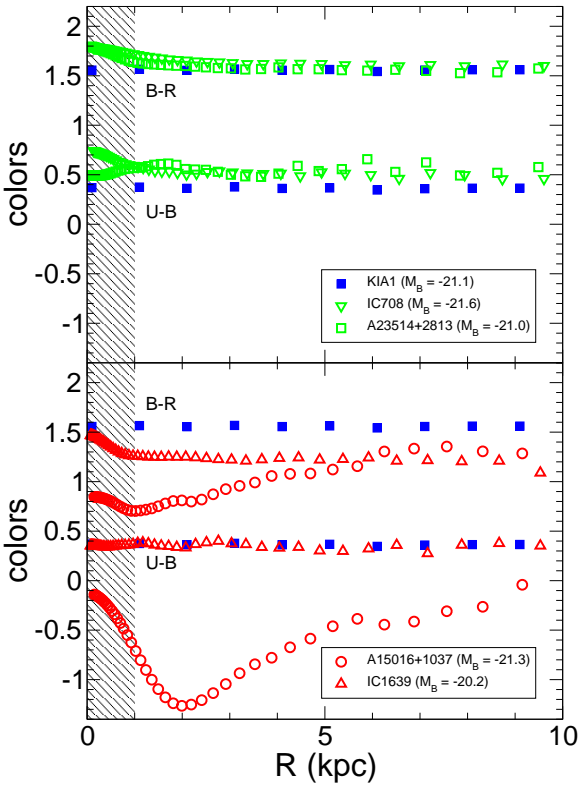


FIG. 6.— $U - B$ and $B - R$ color profiles for the simulated galaxy, compared with those of the “normal” (top panel) and “compact” (bottom panel) ellipticals shown in Figure 5. Observational data is from Jansen et al. (2000).

$\epsilon = 1 - b/a \approx 0.1$ when seen face-on to a maximum ellipticity of $\epsilon \approx 0.4$ when seen edge-on. The stellar distribution is thus only mildly triaxial, with axis ratios of order 1:0.9:0.6. This is confirmed by the good alignment between the projected photometric and kinematic principal axes: the maximum misalignment is less than 8 degrees (for the 30° panel in Figure 7).

As is clear from the velocity maps in Figure 7, the galaxy has a well defined sense of rotation, and a shape in projection that is closely linked to the apparent degree of rotational support. The velocity difference at $R = 2 R_e$ varies from 134 km s $^{-1}$ for a 10 degree inclination to 468 km s $^{-1}$ when projected edge-on. This is the kinematic signature expected for an oblate rotator whose shape is mainly determined by rotation; a result confirmed by Figure 8, where we plot the apparent ellipticity of the galaxy versus the ratio between the apparent rotation speed and the velocity dispersion, V_{rot}/σ , measured at $R = R_e$. The solid squares correspond to the different projections shown in Figure 7. The thick solid line in Figure 8 corresponds to an “oblate rotator” where rotation dictates the shape of the stellar distribution (see Figure 4-6 of Binney & Tremaine 1987). The agreement between the solid line and the solid squares provides strong evidence for the importance of rotation in the structure of the simulated galaxy. The open symbols in Figure 8 illustrate the well known result that rotation plays an important role in faint ellipticals (open triangles) and that rotational support becomes increasingly weak with luminosity.

The importance of rotation in the simulated galaxy is somewhat unexpected, as it is usually taken to imply that a large fraction of the stars have formed following a smooth dissipative collapse. In this case, however, the formation of 95% of the stars predate the final major (1:3) merger at $z \sim 0.6$ which transforms the two progenitor disks into a spheroid. Only 3% of the stars form during the merger event. Simple oblate rotators can apparently form even under circumstances as inauspicious as a major merger.

The reason why the merger remnant structure is so kinematically simple—despite its violent assembly history—appears to be linked to couplings between the internal structure of the progenitor disks and the orbital parameters of the merger. Indeed, both disks rotate prograde relative to the orbit of the encounter, and their inclination with respect to the orbital plane is modest (18° in one case, 2° in the other). This reflects a high degree of coherence between scales during the torquing process that endowed the progenitors, as well as the remnant, with net angular momentum.

It is difficult to conclude from a single example whether this cosmologically-induced coincidence between rotation on small and large scales is actually responsible for the structural simplicity of elliptical galaxies. If confirmed, however, it would help to remove one major objection to the merger model of elliptical galaxy formation: that dissipationless mergers lead to highly triaxial remnants with kinematic structure too peculiar to be consistent with observation (Barnes 1992; Hernquist 1992, 1993). A formation scenario where major mergers play an important role in the formation of all spheroid-dominated galaxies, and where the amount of dissipation involved decreases systematically with luminosity appears thus a viable way of accounting for the gross morphological and dynamical properties of ellipticals.

3.2.4. Boxy and disky isophotal shapes

Although the isophotes shown in Figure 7 are well approximated by ellipses, small but significant deviations from perfect ellipsoidal shapes are also robustly measured. Of particular interest is the a_4 parameter, which measures $m = 4$ deviations from perfect ellipses: $a_4 < 0$ signals “boxy” isophotes whereas $a_4 > 0$ imply “disky” deviations from perfect ellipses (Bender & Möllenhoff 1987). Observationally, there is a clear trend between a_4 and the degree to which the galaxy’s shape is supported by rotation. Disky isophotes are typically associated with fast rotators, whereas boxy ellipticals are most often those exhibiting little rotation (see, e.g., open symbols in Figure 10). Given that rotational support decreases with luminosity (§ 3.2.3) it is somewhat surprising that a_4 correlates only weakly with luminosity, as seen in Figure 11. One reason for this is that a number of fast-rotating ellipticals have boxy isophotes, apparently at odds with the simple interpretation that disky isophotes are the result of a dissipative collapse phase responsible for the galaxy’s rotational support.

Our simulation offers a tentative explanation for these trends. Figure 9 shows a_4 as a function of radius, computed for the various projections shown in Figure 7. The triaxial nature of the stellar component results in a_4 values that vary substantially with inclination and radius. Near the center (i.e., for $R \lesssim 0.5 R_e$), $a_4 \sim 0$, a result which is possibly associated with smoothing of the image and of the gravitational potential; a circle of radius $\sim 0.5 R_e$ is of order the gravitational softening and spans only 34 pixels. Further from the center, however, a more clearly discernible inclination-dependent trend emerges: at the effective radius, isophotes are boxy ($a_4 < 0$)

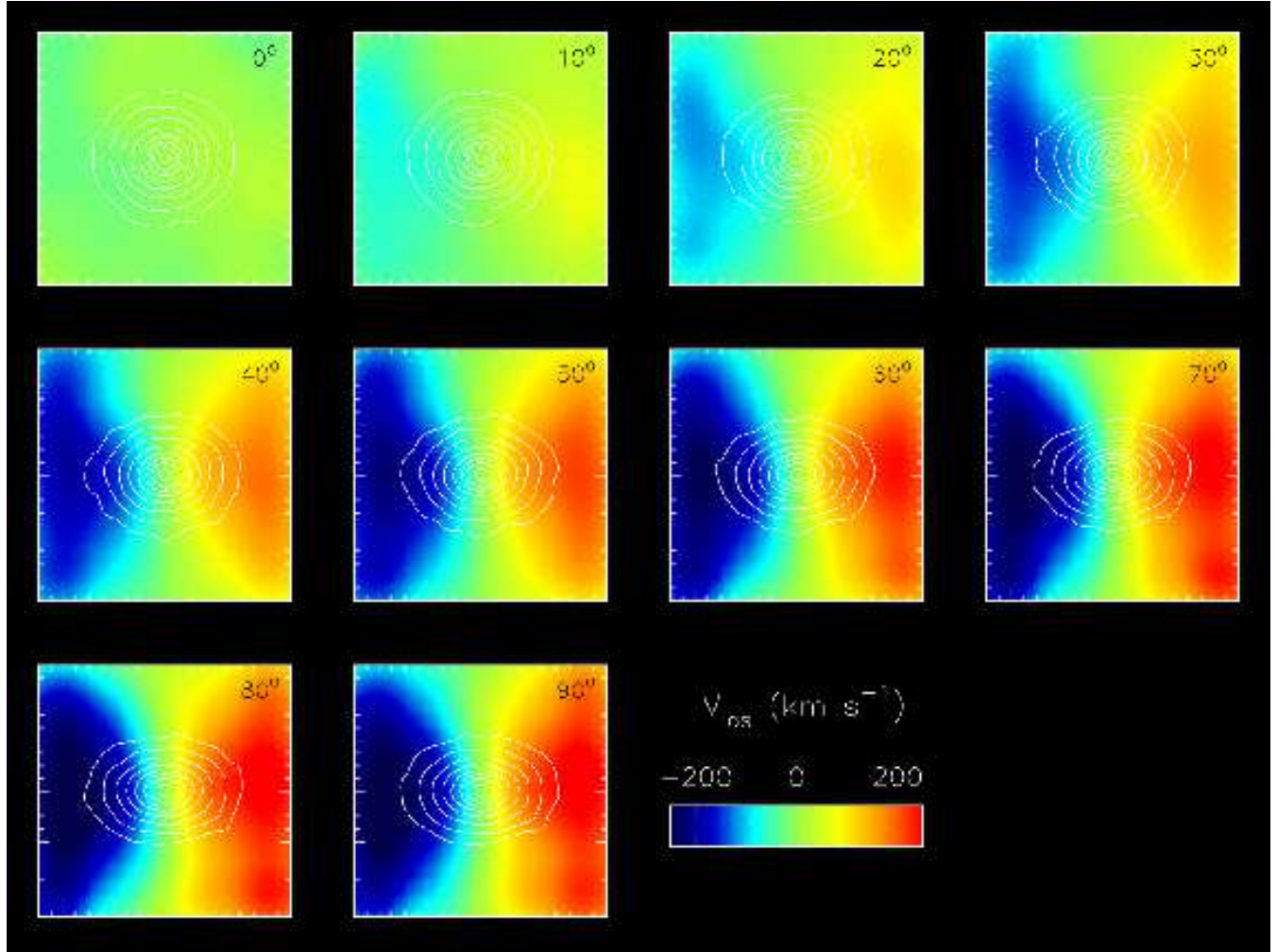


FIG. 7.— Line-of-sight velocity maps and isophotal structure of the simulated galaxy, measured for ten different projections from 256×256 -pixel images constructed using all star particles in a box of 10 kpc on a side. The image is smoothed with a 0.5-kpc Gaussian filter matching the gravitational softening length. Ellipses are fit to these isophotes using the ISOPHOTE routine within the STSDAS package of IRAF. Orientations are chosen so that the projected major axis is aligned horizontally in each image. Note the good agreement between the photometric and kinematic axes, reflecting the very mild triaxial structure of the simulated galaxy.

when the galaxy is seen at low inclinations but the trend reverses sign for higher inclinations; disk-like isophotes ($a_4 > 0$) are seen when the galaxy is projected nearly edge-on. A trend between a_4 and rotation support thus results, as illustrated by the solid squares in Figure 10. This figure shows that boxy isophotes may be obtained even when V_{rot}/σ approaches values as high as those of an oblate rotator; i.e., boxy isophotes may occur even in systems where rotational support plays an important role.

We end this discussion with a caveat: the isophotal deviations from perfect ellipses measured for KIA1 are statistically very significant, but they are also small, and cover a dynamic range smaller than observed. In particular, the maximum “diskiness” measured in KIA1 is of order $\sim 1\%$, compared to the 4% reaches in some low-luminosity systems (Figure 10). Also, the maximum “boxiness” in KIA1 does not exceed $a_4 \sim -0.5\%$; whereas $a_4 < -1\%$ is not unusual in observational samples. As our simulated sample grows, we expect to be able to elucidate better these trends and to provide insight into the meaning of the correlations (or lack thereof) between shape, kinematics, and photometry within the hierarchical merger model for the formation of ellipticals.

3.3. Kinematical Properties

3.3.1. Circular velocity profiles

The kinematics of the luminous component of the galaxy is largely dictated by the mass distribution, which may be expressed by the circular velocity profile, $V_{\text{circ}}(r) = (GM(r)/r)^{1/2}$. This is shown in Figure 12, and indicates that the luminous (stellar) component dominates strongly the mass distribution near the center. Indeed, the stellar component outweighs the dark matter by as much as 3 to 1 at the effective radius and by roughly 1.9:1 as far away as $5 R_e$ (~ 7 kpc) from the center. Only beyond 17 kpc does the dark matter begin to dominate the mass budget in the galaxy.

The high concentration of the stellar component results in large circular velocities near the center; at the effective radius the circular velocity exceeds 700 km s^{-1} . The circular velocity declines steeply with radius; at 8 kpc from the center it comes down to just $\sim 450 \text{ km s}^{-1}$. At face value, this is at odds with the results of Gerhard et al. (2001), who find that the circular velocity profile of normal ellipticals— inferred from their line of sight absorption line profiles—is approximately flat, varying by less than 10% between $\sim 0.2 R_e$ and

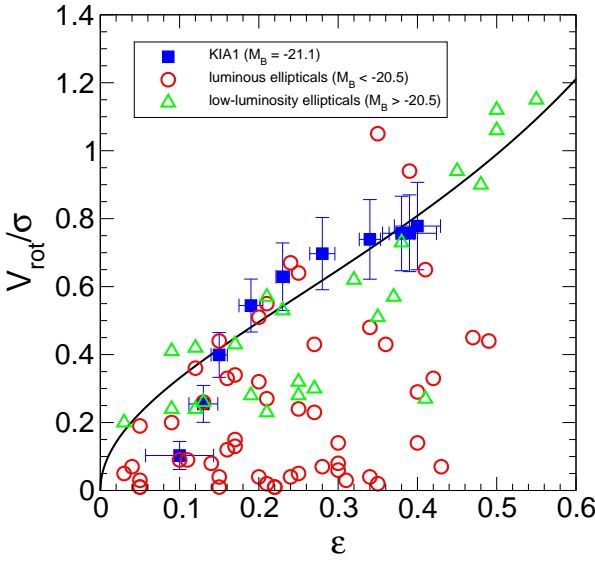


FIG. 8.— The rotation measure, V_{rot}/σ , plotted versus the ellipticity of the galaxy. Both quantities are computed at the effective radius. Solid squares correspond to the same 10 projections shown in Figure 7. Open circles and triangles correspond to ellipticals brighter and fainter than $M_B = -20.5$, respectively. The solid line indicates the relation expected for an oblate rotator whose shape is determined by the degree of rotational support [see Figure 4-6 of Binney & Tremaine (1987)].

$\sim 2 R_e$.

Although this discrepancy seems worrisome, one should recall that the simulated galaxy resembles photometrically a compact elliptical (§ 3.2.1); a relatively rare class not well represented in Gerhard et al.’s sample. Indeed, the only compact elliptical in their dataset is M87’s companion NGC4486B, which is referred to by these authors as “exceptional in almost all respects” (see also Prugniel, Nieto, & Simien 1987; Peletier 1993). The inset in Figure 12 compares the inner circular velocity profile of KIA1 with that derived by Gerhard et al. (2001) for NGC4486B, each scaled to the same maximum circular speed and plotted only as far as $2.5 R_e$. The circular velocity profile of NGC4486B is clearly declining and, over this limited radial range, it does not differ dramatically from that of KIA1. This is perhaps unsurprising given the photometric evidence: the central dynamics of such highly concentrated galaxies is solidly dominated by the luminous component, with a negligible contribution from the dark matter component. The sharply concentrated surface brightness profile thus leads to circular velocities that decline steeply with radius. In less concentrated ellipticals the dark matter contribution to the mass profile is proportionally higher, and leads to the “flat” circular velocity curves reported by Gerhard et al. (2001).

3.3.2. Line-of-sight velocity profiles

The shape of absorption line profiles contains unique information about the orbital structure of stars in elliptical galaxies and about the radial dependence of the gravitational potential. They have been profitably used in a number of studies to demonstrate the presence of dark matter within the luminous radius of some elliptical galaxies (Carollo et al. 1995;

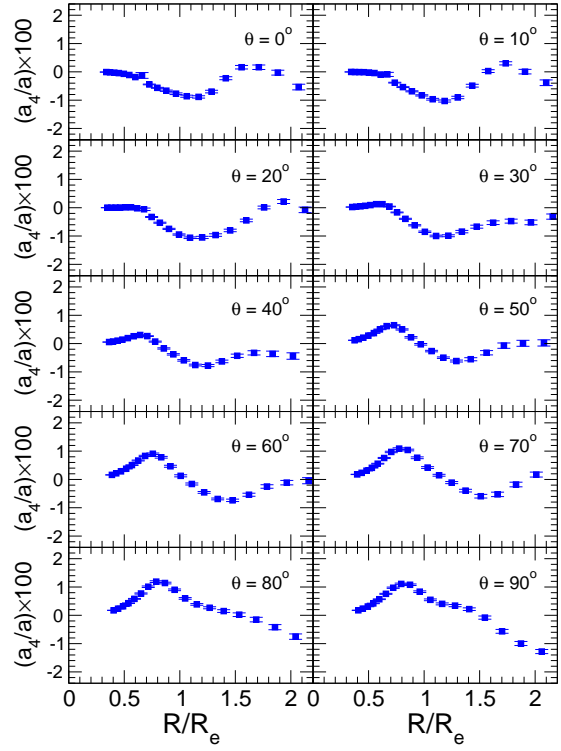


FIG. 9.— The parameter, a_4 , measuring isophotal deviations from perfect ellipses, plotted as a function of projected radius for the same 10 projections shown in Figure 7. Low inclination angles, corresponding to when the galaxy is seen nearly face-on, are characterized by “boxy” ($a_4 < 0$) isophotes, a trend that reverses for higher inclinations. Predominantly “disky” ($a_4 > 0$) isophotes are seen when the galaxy is projected nearly edge-on.

Rix et al. 1997; Gerhard et al. 1998; Kronawitter et al. 2000), as well as to estimate the degree of orbital anisotropy affecting the global dynamics of spheroid-dominated galaxies. Much of this information comes from small but significant departures from Gaussianity in the velocity distribution of stars along the line of sight. These deviations are usually quantified by approximating the line-of-sight velocity distribution (LOSVD) with a Gauss-Hermite series (van der Marel & Franx 1993). The dimensionless h_4 coefficient of this series quantifies kurtosis-like deviations, whilst the h_3 coefficient provides a dimensionless measure of the skewness of the distribution.

We have measured LOSVDs in the simulated galaxy by binning particles along a slit placed on the major axis of different projections of the simulated galaxy. The bin size is adjusted so as to keep a roughly constant number of particles within each bin. Fits using a Gauss-Hermite series to the LOSVDs measured at four different radii along the major axis of an edge-on projection of the galaxy are shown in Figure 13. As seen in this figure, the velocity distributions are very nearly Gaussian, although small but significant deviations are also robustly measured, as quantified by the h_3 and h_4 parameters listed in each panel of Figure 13.

The radial dependence of the kinematic structure is synthesized in the V_{rot} , σ , V_{rot}/σ , h_3 , and h_4 profiles shown in Figure 14 for the case of face-on and edge-on projections, respectively. This figure highlights a number of interesting trends.

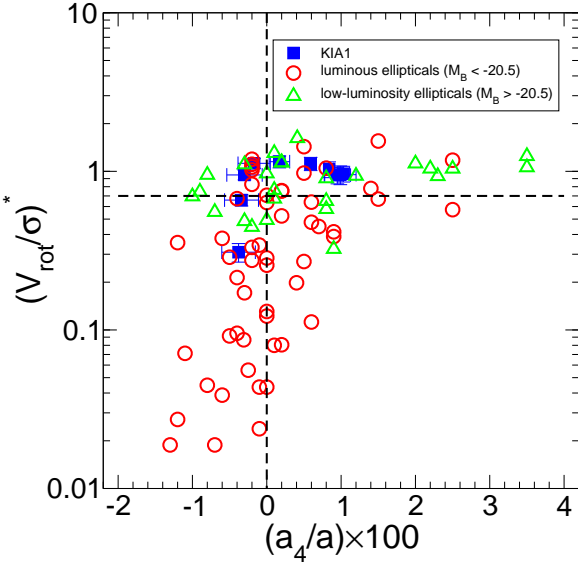


FIG. 10.— Isophotal deviations, as measured by the a_4 parameter at the effective radius, plotted versus the rotational parameter $(V_{\text{rot}}/\sigma)^*$ defined as the ratio between V_{rot}/σ and the value corresponding to an oblate rotator of the same apparent ellipticity. Solid squares correspond to the same 10 projections of the simulated galaxy shown in Figure 7. Open symbols correspond to observed ellipticals from the sample of Bender et al. (1992). The simulated galaxy seems to follow roughly the trend between rotation support and diskiness (boxiness) present in the observations.

The first one is that the importance of rotation is a strong function of radius: when seen edge-on, V_{rot}/σ is of order ~ 0.6 at the smallest radius confidently resolved in the simulation ($R \sim 0.5 R_e$) and reaches roughly unity at $R \sim 1.5 R_e$. This is in agreement with earlier work, which found that the outer regions of merger remnants contain a disproportionate fraction of the angular momentum of the system (Hernquist 1992, 1993).

Two further interesting trends are apparent in Figure 14: (i) h_4 appears to remain positive at essentially all radii, and (ii) the sign of h_3 seems to anti-correlate with that of V_{rot}/σ . The first trend implies that LOSVDs are slightly “boxier” than Gaussian, a clear signature of the importance of tangential motions in the outer regions of the galaxy (Gerhard 1993; van der Marel & Franx 1993). This is confirmed by the solid squares in the bottom panel of Figure 15, where we show the values of h_4 measured on all bins along the major axis of the same 10 projections shown in Figure 7: most h_4 values are found to be positive. This trend, however, is not reproduced in the dataset of Bender et al. (1994) (open circles in Figure 15), who find essentially no correlation between h_4 and V_{rot}/σ , and that h_4 in ellipticals is as likely to be positive as it is to be negative. We interpret this as reflecting the greater variety of structures prevalent in normal ellipticals; i.e., not all can be well approximated by simple oblate rotators. Given that we have a single example, it is not clear how serious this “deficiency” in the model really is; a statistically significant number of simulations is needed before a more definitive characterization of this result may emerge.

On a more optimistic note, the correlation between h_3 and V_{rot}/σ noted above (and shown in more detail in the top

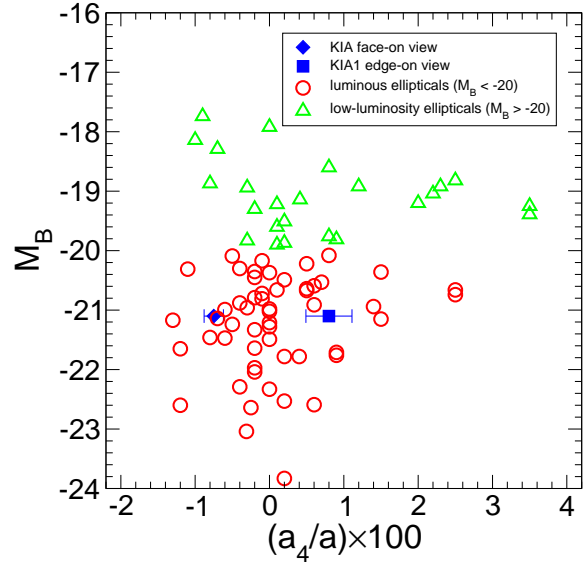


FIG. 11.— Isophotal deviations, as given by the a_4 parameter measured at about the effective radius, plotted versus the absolute magnitude in the B band. A (weak) trend is seen in observational samples for fainter galaxies to have diskier isophotes than their brighter counterparts. The solid symbols illustrate the location of the simulated galaxy, projected so as to be seen edge-on and face-on. There is no obvious disagreement between the isophotal deviations measured in KIA1 and in ellipticals of similar luminosity.

panel of Figure 15) reproduces a well-established observational trend: the asymmetry in the LOSVD is typically such that the excess “tail” in the distribution points to the “origin” of the velocity axis (see, e.g., Figure 13). This asymmetry signals the importance of coherent rotation in the dynamical structure of the galaxy; a similar asymmetry would result from a thick rotationally supported disk and has been used, for example, to argue for massive gaseous disks as responsible for the velocity structure observed in damped Ly- α systems (Prochaska & Wolfe 1998; see, however, Haehnelt, Steinmetz & Rauch 1998 for a different interpretation).

As shown in the top panel of Figure 15, the trend in the simulated galaxy follows the observed one but is less pronounced than reported by Bender et al. (1994): at $|V_{\text{rot}}/\sigma| \sim 1$ Bender et al. find $|h_3| \sim 0.12$ whereas we find $|h_3| \sim 0.03$ for KIA1. Despite this, it is important to note that the sign of the observed trend is reproduced in the simulation, in particular since dissipationless merger simulations have consistently had difficulty reproducing this trend (Naab & Burkert 2001). Our simulation shows that the mild dissipation that accompanies the merger event at $z = 0.6$, together with the large scale couplings between the internal spin of the progenitors and the orbital angular momentum of the collision, may be enough to reconcile such trend with hierarchical merger models of elliptical galaxy formation.

3.4. The Fundamental Plane

A powerful diagnostic of the success of simulations in reproducing the observed properties of galaxies results from comparing their luminosity, size, and characteristic velocity with the scaling relations linking these properties in galaxies of various types. The most significant of these relations

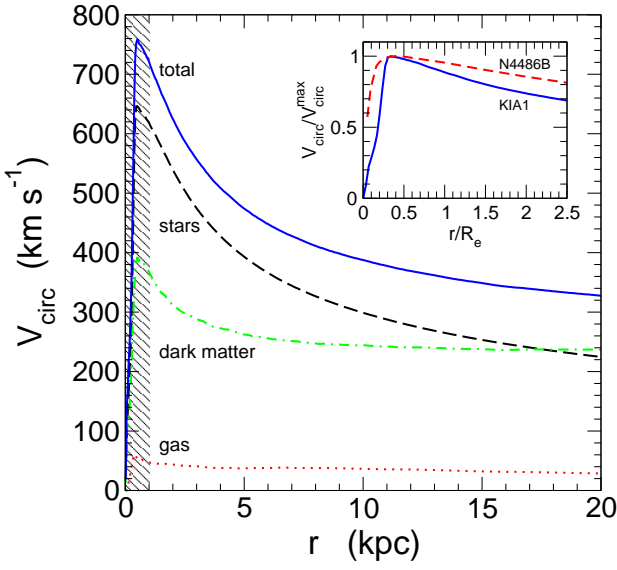


FIG. 12.— Circular velocity profile of the simulated galaxy (solid line), together with the contributions from the stellar (dashed), dark matter (dot-dashed), and gas (dotted) components, respectively. The stellar component dominates over the dark matter as far out as ~ 17 kpc from the center. The circular velocity profile declines steadily from the center outwards, at odds with the results of Gerhard et al. (2001) for normal ellipticals, but in closer agreement with the profile of “compact” ellipticals. The inset compares the inner circular velocity profile of KIA1 with the declining profile derived by Gerhard et al. for the compact elliptical NGC4486B (dashed line). Both profiles have been scaled to the maximum circular velocity for ease of comparison.

for elliptical galaxies is the “Fundamental Plane” (Djorgovski & Davis 1987), or its equivalent, the $D_{n-\sigma}$ relation (Dressler et al. 1987) assiduously used in extragalactic distance scale studies.

The Fundamental Plane (FP) describes the relation between effective radius (R_e), effective mean surface brightness ($\langle \mu \rangle_e$), and central velocity dispersion (σ_0) of early-type galaxies. Clusters and field ellipticals are found to populate a thin plane in this three-dimensional space, slightly “tilted” relative to the plane expected from the virial theorem, as applied to homologous systems;

$$\log R_e = 2(\log \sigma_0 + 0.2 \langle \mu \rangle_e) - \log(\Upsilon/\Upsilon_0) + \text{constant}, \quad (1)$$

or, equivalently,

$$\log \sigma_0 = \frac{1}{2}(\log R_e - 0.4 \langle \mu \rangle_e) + \frac{1}{2} \log(\Upsilon/\Upsilon_0) + \text{constant}. \quad (2)$$

The solid line in Figure 16 indicates the loci expected for systems that follow strictly the homologous virial scaling, after choosing the reference dynamical mass-to-light ratio, Υ_0 , so as to bisect the normal ellipticals in the sample (shown as open circles). Galaxies to the left of this line have mass-to-light ratios $\Upsilon > \Upsilon_0$; those to the right have $\Upsilon < \Upsilon_0$. The tight trend shown in Figure 16 suggests that the Fundamental Plane is largely a reflection of the virial relations, modulated by relatively minor variations in mass-to-light ratio. This is confirmed by the fact that the best fitting “plane” through the

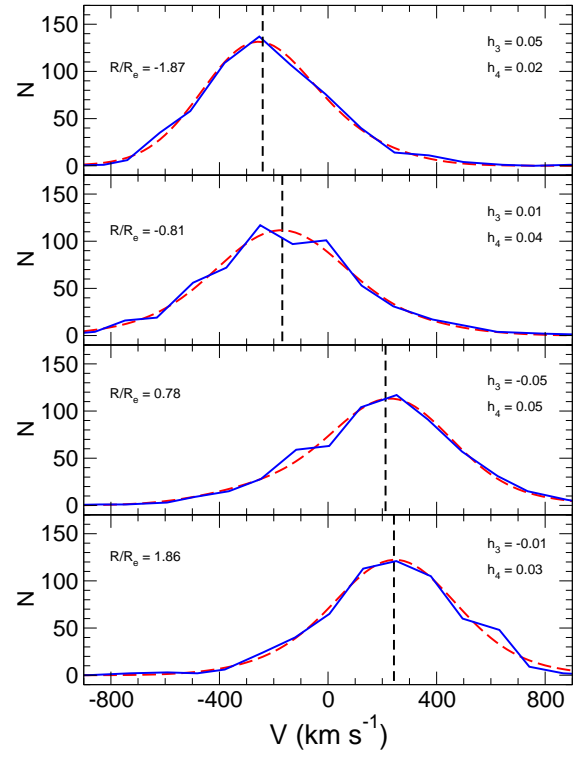


FIG. 13.— Line-of-sight stellar velocity profiles, measured at different radii along the major axis of an edge-on projection of the simulated galaxy (solid lines). Dashed lines show the best Gauss-Hermite polynomial fit, with parameters h_3 and h_4 as listed in each panel. Note the anti-correlation in sign between h_3 and the mean velocity. See text for further discussion.

dataset shown in Figure 16 is

$$\log R_e = 1.25(\log \sigma_0 + 0.26 \langle \mu \rangle_e) - 9.009 \quad (3)$$

(Bender et al. 1998). Comparing the quantities between parentheses in the right-hand side of equations (1) and (3) confirms that the observed scaling of effective radius with velocity dispersion and surface brightness is very similar to the virial scaling.

The distribution of normal ellipticals (open circles) around the solid line in Figure 16 illustrates the well-known fact that the dynamical mass-to-light ratio varies systematically with luminosity in such systems; large (luminous) ellipticals have higher dynamical mass-to-light ratios than smaller (fainter) systems. The spread in mass-to-light ratios is, however, relatively small; most systems, including morphologically distinct galaxies such as “bright dwarf ellipticals”, and “compact ellipticals” (following the nomenclature of Bender et al. 1992), lie between the dashed and dot-dashed lines in Figure 16, and therefore have mass-to-light ratios that differ from Υ_0 by less than a factor of 2.

In order to situate the simulated galaxy (KIA1) within this plane, we need to estimate its central velocity dispersion, σ_0 , within an aperture comparable to that used in observations, typically less than about half the effective radius. Unfortunately, velocities within such small radii ($\lesssim 0.7$ kpc) in the simulated galaxy are significantly affected by the gravitational softening; note, for example, the (artificial) central dip in σ shown in Figure 14. We have therefore chosen to estimate σ_0

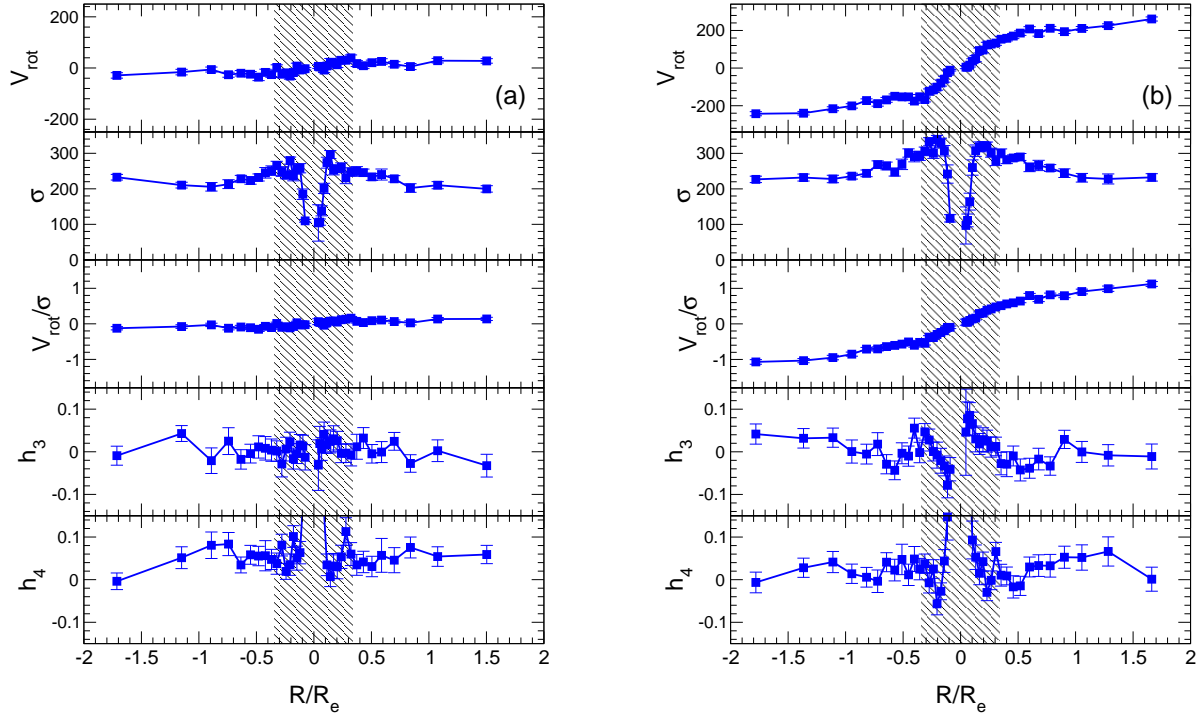


FIG. 14.—Kinematics of the simulated galaxy measured along the major axis of the (a) face-on and (b) edge-on projections. From top to bottom, each panel shows: the mean velocity V_{rot} ; the velocity dispersion σ (both in km s^{-1}); the rotational support measure V_{rot}/σ ; as well as the h_3 and h_4 Gauss-Hermite parameters. The projected radius R is normalized to the effective radius R_e . Shaded area marks the region likely compromised by the gravitational softening.

using a de Vaucouleurs model matched to have the same photometric parameters and to enclose the same total mass within the effective radius as KIA1. This yields a central velocity dispersion of $\sigma_0 \approx 650 \text{ km s}^{-1}$, a factor of ~ 2.7 higher than would be estimated without accounting for this correction.

Adopting this value of σ_0 , the simulated galaxy sits slightly to the left of the virial scaling in Figure 16, implying a dynamical mass-to-light ratio of order $\Upsilon \sim 2 \Upsilon_0$. This is comparable to that of luminous ellipticals. Indeed, within one effective radius, $R_e = 1.32 \text{ kpc}$, the total mass is $M_{\text{tot}}(r < R_e) = 1.45 \times 10^{11} M_\odot$, which, combined with a total luminosity of $L_B = 4.16 \times 10^{10} L_\odot$, results in a total mass-to-light ratio of order $\Upsilon_B(R_e) \sim 3.5$ in solar units, comfortably within the range estimated by Gerhard et al. (2001; see their Figure 13). In other words, the unremarkable mass-to-light ratio of KIA1 is responsible for its proximity to the Fundamental Plane seen edge-on.

This result is confirmed in Figure 17, which shows another nearly edge-on projection of the Fundamental Plane. The lines in this Figure correspond to the virial scaling expressed in equation (2), and use the same normalization as those in Figure 16. Figure 17 shows that KIA1 clearly stands out from the rest: its velocity dispersion, indeed, is far higher than that of normal ellipticals of similar luminosity. KIA1 also stands out in terms of its surface brightness, as is clear from the nearly face-on view of the Fundamental Plane shown in Figure 18. The surface brightness of KIA1 is comparable to those of the M32-like group of compact ellipticals, one example of which is NGC4486B.

As KIA1, NGC4486B differs from normal ellipticals not only in surface brightness; it also has a much higher velocity

dispersion and circular velocity than ellipticals of similar luminosity (see, e.g., Kronawitter et al. 2000 and Gerhard et al. 2001). This is shown in Figure 19, where we compare KIA1 and NGC4486B with the “Tully-Fisher relation” of normal ellipticals derived by Gerhard et al. (2001). As for spirals, this relation links the total luminosity of the galaxy to the (maximum) circular velocity of the system, obtained by Gerhard et al. through detailed analysis of radially-resolved absorption line profiles.

Both NGC4486B and KIA1 deviate strongly from the Tully-Fisher relation of normal ellipticals: they have circular speeds a factor of 3-4 higher than normal ellipticals of comparable luminosity. This seems consistent with the photometric evidence. Ellipticals as bright as KIA1 have effective radii typically of order $\sim 10 \text{ kpc}$, a factor of ~ 10 times larger than KIA1. Assuming similar stellar mass-to-light ratios and, as seems likely, that the dark matter plays a minor role within the effective radius, this implies that KIA1 should have a circular velocity $\sim \sqrt{10} \approx 3.2$ times higher than average, in good agreement with the result shown in Figure 19. In other words, the Tully-Fisher relation for ellipticals derived by Gerhard et al. (2001) only applies to ellipticals of “normal” surface brightness, and large deviations from this relation are expected for systems whose surface brightness deviates strongly from the norm. It would be interesting to confirm this assertion by extending the same kind of analysis performed by Gerhard et al. to a sample of compact ellipticals.

Finally, the comparison shown in Figure 19 also suggests that the higher concentration of the luminous component may be one major reason why ellipticals of similar luminosity have higher circular speeds than spirals. The higher the surface

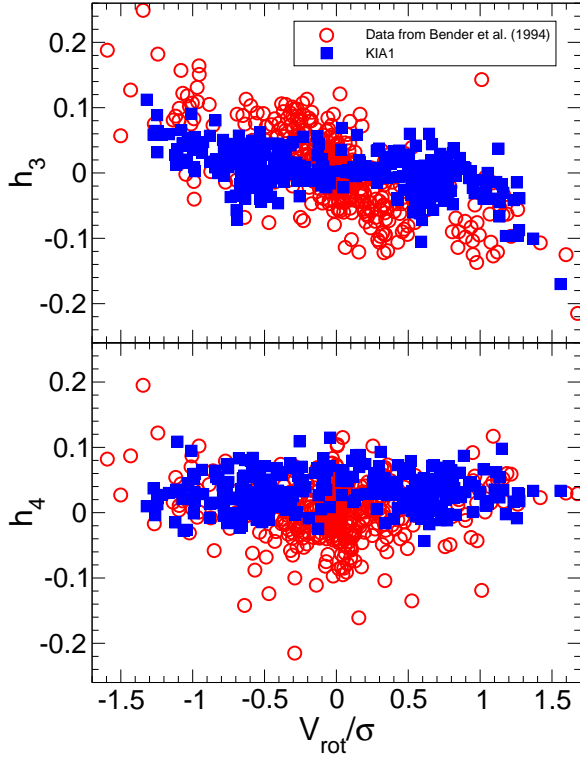


FIG. 15.— Gauss-Hermite parameters h_3 and h_4 plotted as a function of V_{rot}/σ , measured along the major axis of the same 10 projections shown in Figure 7 (solid squares). Open circles correspond to data from Bender et al. (1994). Note that the trend between h_3 and V_{rot}/σ is reproduced in the simulated galaxy. See text for further discussion.

brightness the more important the luminous component in the dynamics of the system and the higher the circular velocity of the system. In this interpretation, compact ellipticals offer a rare glimpse at systems where dark matter plays a negligible dynamical role within the luminous radius. If confirmed, this property would make them ideal testbeds for models that attempt to constrain the stellar mass-to-light ratio (and by extension other properties such as the stellar Initial Mass Function) of spheroid-dominated galaxies.

4. SUMMARY

We present a detailed analysis of the dynamical and photometric properties of an elliptical galaxy simulated in the Λ CDM scenario. The simulation includes the gravitational and hydrodynamical effects of dark matter, gas and stars. Star formation is modeled through a simple recipe that transforms cold, dense, locally-collapsing gas into stars at a rate controlled by the gas density. Energetic feedback from stellar evolution is calibrated to match observed star formation rates in isolated disk galaxy models, but in a form that minimizes the kinetic coupling between feedback energy and the interstellar medium. As a result, there is little modulation of the star formation rate, which tracks closely the rate at which gas cools and condenses at the center of dark matter halos.

Our main results may be summarized as follows:

1. The galaxy is assembled through a number of high-redshift mergers followed by brief periods of quiescent

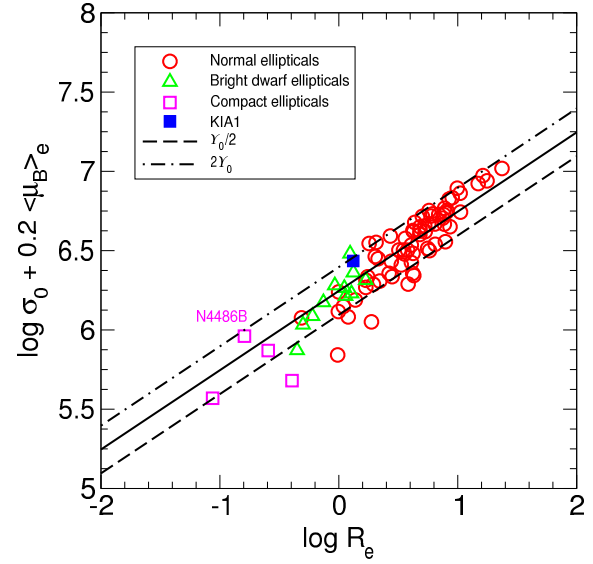


FIG. 16.— Nearly edge-on projection of the Fundamental Plane. Open symbols are data from Bender et al. (1992). Each symbol corresponds to a different morphological “class” of elliptical galaxy, as labeled in the figure. Homologous systems obeying the virial theorem and of constant mass-to-light ratio are expected to populate lines of slope $1/2$ in this plane, as shown by the solid line. Horizontal deviations from this line may be ascribed to varying dynamical mass-to-light ratio, Υ . The dashed and dot-dashed lines correspond, respectively, to systems with $1/2$ and 2 times the fiducial mass-to-light ratio parameter Υ_0 chosen to draw the solid line. See text for interpretation.

accretion which culminate in a major (1:3) merger at $z \sim 0.6$. Star formation progresses swiftly in early collapsing progenitors and accelerates during mergers, only weakly impeded by our choice of feedback parameters; 50% of the present-day stars have already formed by $z \sim 2.4$ and 75% of them by $z \sim 1.3$.

2. The merger at $z = 0.6$ mixes the stars of the two disk progenitors into a highly concentrated spheroidal component that dominates the galaxy dynamically and photometrically at $z = 0$. Few stars form after this event, and the surface brightness profile of the galaxy at $z = 0$ can be reasonably fit with an $R^{1/4}$ law. The effective radius of the simulated galaxy is $R_e \sim 1.32$ kpc, smaller by a factor of 4-8 than that of normal ellipticals of similar luminosity. The surface brightness profile of the simulated galaxy thus resembles that of the less common class of M32-like “compact” ellipticals, although it is far brighter than most and is not a satellite of brighter galaxies.
3. The luminosity (mass) weighted age of the stars in the galaxy is 10.0 (10.9) Gyrs, which leads to red colors consistent with normal ellipticals of similar luminosity, $B - R \sim 1.6$. The late merger that shapes the spheroid mixes stars very efficiently and results in very weak color gradients, in agreement with observations.
4. The luminous component dominates the structure of the simulated galaxy out to ~ 13 effective radii, imposing

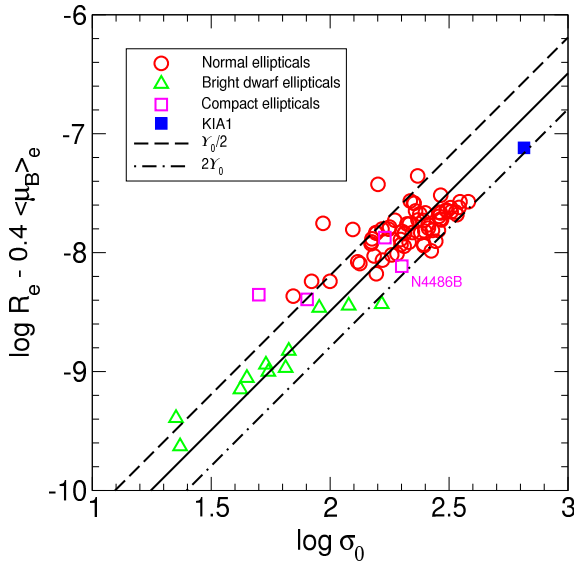


FIG. 17.— Another nearly edge-on projection of the Fundamental Plane. The axis of the figure are chosen, as in Figure 16, so that homologous systems of constant mass-to-light ratio obeying the virial theorem align themselves along lines parallel to the solid line in the figure, drawn for a fiducial value of the dynamical mass-to-light ratio, Υ_0 . Departures to the right or left of this line may be ascribed to $\Upsilon > \Upsilon_0$ or $\Upsilon < \Upsilon_0$, respectively. See text for interpretation.

a clearly declining circular velocity profile: the circular velocity drops from 748 km s^{-1} at $r = 0.5 R_e = 0.66 \text{ kpc}$ to 578 km s^{-1} at $r = 2 R_e = 2.64 \text{ kpc}$. Such sharp decline is at odds with the roughly flat circular velocity curve of normal ellipticals inferred from detailed modeling of radially-resolved dynamical observations (Gerhard et al. 2001). However, it appears to be consistent with the mass profile inferred for compact ellipticals such as NGC4486B.

5. Kinematically, the simulated galaxy resembles an E4 oblate rotator where rotation support increases sharply with radius: when seen edge-on, V_{rot}/σ increases from 0.6 at $r = 0.5 R_e = 0.66 \text{ kpc}$ to 1.1 at $r = 1.5 R_e = 1.98 \text{ kpc}$. The galaxy is only mildly triaxial; its average axis ratios, as measured from the stellar inertia momentum tensor within $2 R_e$ are $b/a \sim 0.9$ and $c/a \sim 0.6$. These results reflect the importance of dissipation as well as of couplings between the internal dynamics and orbital parameters of the merger progenitors. The smooth and kinematically ordered structure of the simulated galaxy thus lifts (or at least eases) some of the objections to a merger origin of ellipticals raised by the highly triaxial structure of the remnants of early dissipationless merger simulations (Barnes 1992; Hernquist 1992).
6. Isophotes are well approximated by ellipses, with only a weak radial variation in position angle and ellipticity. Small but significant deviations from perfect ellipses are also measured; the simulated galaxy appears “boxy” ($a_4 < 0$) when seen face-on and “disky” ($a_4 > 0$) when

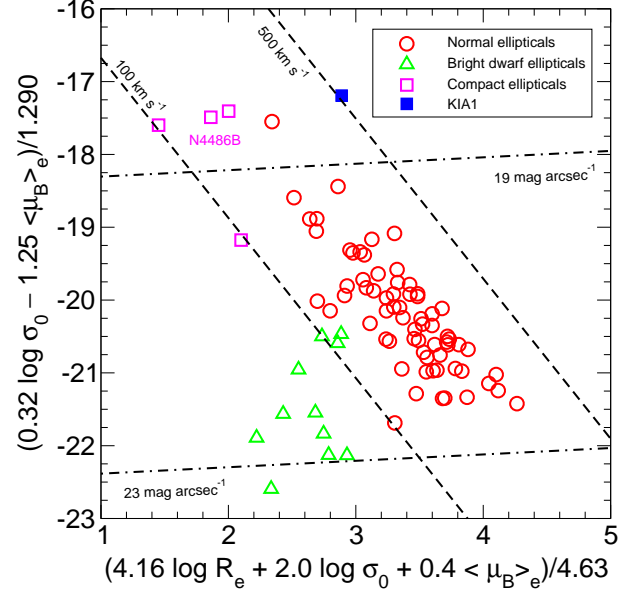


FIG. 18.— Nearly face-on view of the Fundamental Plane, chosen to be orthogonal to the projections shown in Figures 16 and 17. Surface brightness increases vertically in this plane, and shows that the simulated galaxy has a much higher surface brightness than normal ellipticals of comparable luminosity.

seen edge-on. This appears consistent with the weak correlation observed between apparent rotation and the sign of the a_4 parameters: boxy ellipticals appear to rotate much more slowly than their disk-like counterparts.

7. The line-of-sight velocity distribution of stars (LOSVD) is approximately Gaussian, although small departures from Gaussianity that reflect the importance of ordered rotation are also robustly measured. The Gauss-Hermite coefficient h_4 tends to be positive and the sign of the h_3 parameter (anti)correlates with that of the mean velocity. These trends are reasonably consistent with observation and differ from those found in earlier dissipationless merger simulations, again alleviating serious objections to the merger origin of ellipticals raised by earlier work (see, e.g., Naab & Burkert 2001 and references therein).
8. Despite its high concentration, the simulated elliptical lies close to edge-on projections of the Fundamental Plane. This implies a dynamical mass-to-light ratio comparable to those of normal ellipticals. On the other hand, due to its high surface brightness, the circular velocity (and velocity dispersion) of the simulated galaxy far exceeds that of normal ellipticals of similar luminosity. It thus clearly stands out, as other compact ellipticals, from the rest of spheroid dominated galaxies in face-on projections of the Fundamental Plane or in other scaling relations such as the Tully-Fisher relation.

Overall, the simulation described here shows that a hierarchical merging process that includes dissipation and star formation is a promising way of accounting for many of the observed structural properties of spheroid-dominated galaxies. Repeated episodes of dissipational collapse followed by

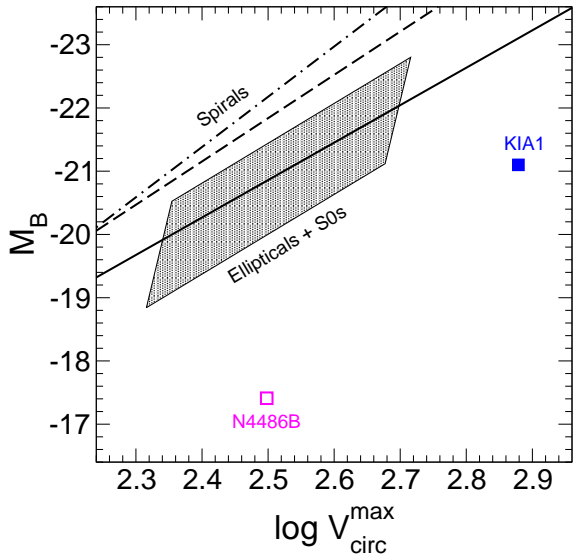


FIG. 19.— The “Tully-Fisher” relation of elliptical galaxies (i.e., the maximum circular velocity plotted versus B -band absolute magnitude), as derived by Gerhard et al. (2001) for a sample of 21 nearly round ellipticals (shaded box), compared with the simulated galaxy (KIA1) and the compact elliptical NGC4486B. Both galaxies deviate strongly from the relation that holds for normal ellipticals. This is consistent with the fact that both NGC4486B and KIA1 are about one order of magnitude smaller than normal ellipticals but have similar stellar mass-to-light ratios.

merger events lead to spheroids that are only mildly triaxial and of relatively simple kinematic structure. This is in better agreement with observation than earlier merger models between stellar disks that neglected dissipation and star formation and eases a number of concerns regarding the viability of merger models for the origin of ellipticals. We see this as a positive step towards reconciling the observed structure of elliptical galaxies with a hierarchical assembly process where mergers play a substantial role.

At the same time, agreement with observation is not perfect: despite its late assembly ($z \sim 0.6$), the stellar component is more centrally concentrated than normal ellipticals. This is intriguing, as it demonstrates that high stellar density does not necessarily imply high redshift of assembly, as is generally assumed in the “monolithic collapse” model (Partridge & Peebles 1967; Peebles 2002). However, we do not consider this to be a robust generic prediction for galaxies forming in Λ CDM halos such as the one under consideration here. Rather, as discussed in earlier papers of this

series (Abadi et al. 2003a,b), it reflects the ineffectiveness of our feedback algorithm at curtailing the efficient cooling of gas and its rapid transformation into stars in dense, early-collapsing progenitors.

Thus, although several compact ellipticals that closely resemble photometrically the simulated galaxy may be found in the Nearby Field Galaxy Survey of Jansen et al. (2000; e.g., IC1639 and A15016+1037), we cannot claim to have identified the mechanism responsible for the phenomenon of compact ellipticals. Still, our preliminary conclusion that such bright compact ellipticals are just “scaled up” versions of M32 (or NGC4486B) requires that they should have extremely high central velocity dispersions, $\sigma_0 \sim 600 \text{ km s}^{-1}$. Observational estimates of σ_0 for these galaxies are as yet unavailable, but they may provide a straightforward way to validate or to rule out some of our conclusions. This is important, since many of the best known examples of compact ellipticals are low-luminosity satellites to bright galaxies, a result that has led to speculation that tides may play an important role in their formation (Faber 1973; Bekki et al. 2001). Should IC1639 and A15016+1037 be confirmed to be in the same class as M32 or NGC4486B would serve to undermine the idea that tidal stripping plays a crucial role in the formation of these systems (see also Nieto & Prugniel 1987; Choi et al. 2002, for other lines of evidence).

It seems clear from this discussion that shedding light on this issue will require further investigation of other star formation/feedback implementations, especially since galaxies with unrealistically high stellar concentration appear to be a general result of the numerical implementation discussed here. Reversing this trend would require a feedback algorithm able to hinder star formation in high-redshift progenitors much more efficiently than in the modeling adopted here. There is indeed preliminary indication that this may actually be possible (Springel 2000; Sommer-Larsen et al. 2002a,b; Croft et al. 2002). At the same time, it is also clear that the physically compelling description of feedback apparently needed is still somewhat beyond reach. Accounting fully for the structure and dynamics of elliptical galaxies in a Λ CDM cosmogony may well have to wait until a proper description of the interaction between energetic feedback processes and the interstellar medium finally emerges.

This work has been supported by grants from the U.S. National Aeronautics and Space Administration (NAG 5-10827), the David and Lucile Packard Foundation, and the Natural Sciences and Engineering Research Council of Canada.

REFERENCES

Abadi, M. G., Navarro, J. F., Steinmetz, M., & Eke, V. R. 2003a, ApJ, 591, 499
 Abadi, M. G., Navarro, J. F., Steinmetz, M., & Eke, V. R. 2003b, ApJ, in press
 Barnes, J. E. 1992, ApJ, 393, 484
 Barnes, J. E. & Hernquist, L. E. 1991, ApJ, 370, L65
 Bekki, K., Couch, W. J., Drinkwater, M. J., & Gregg, M. D. 2001, ApJ, 557, L39
 Bender, R. 1988, A&A, 193, L7
 Bender, R. & Möllenhoff, C. 1987, A&A, 177, 71
 Bender, R. & Nieto, J.-L. 1990, A&A, 239, 97
 Bender, R., Burstein, D., & Faber, S. M. 1992, ApJ, 399, 462
 Bender, R., Saglia, R. P., & Gerhard, O. E. 1994, MNRAS, 269, 785
 Bender, R., Saglia, R. P., Ziegler, B., Belloni, P., Greggio, L., Hopp, U., & Bruzual, G. 1998, ApJ, 493, 529
 Binney, J., & Tremaine, S. 1987, Galactic Dynamics (Princeton, NJ: Princeton University Press)
 Bruzual A., G. & Charlot, S. 1993, ApJ, 405, 538
 Carollo, C. M., de Zeeuw, P. T., van der Marel, R. P., Danziger, I. J., & Qian, E. E. 1995, ApJ, 441, L25
 Choi, P. I., Guhathakurta, P., & Johnston, K. V. 2002, AJ, 124, 310
 Contardo, G., Steinmetz, M., & Fritze-von Alvensleben, U. 1998, ApJ, 507, 497
 Croft, R. A. C., Hernquist, L., Springel, V., Westover, M., & White, M. 2002, ApJ, 580, 634

Davies, R. L., Efstathiou, G., Fall, S. M., Illingworth, G., & Schechter, P. L. 1983, *ApJ*, 266, 41

de Zeeuw, T. & Franx, M. 1991, *ARA&A*, 29, 239

de Zeeuw, P. T. et al. 2002, *MNRAS*, 329, 513

Djorgovski, S. & Davis, M. 1987, *ApJ*, 313, 59

Dressler, A., Lynden-Bell, D., Burstein, D., Davies, R. L., Faber, S. M., Terlevich, R., & Wegner, G. 1987, *ApJ*, 313, 42

Faber, S. M. 1973, *ApJ*, 179, 423

Franx, M. & Illingworth, G. D. 1988, *ApJ*, 327, L55

Franx, M., Illingworth, G., & de Zeeuw, T. 1991, *ApJ*, 383, 112

Gerhard, O. E. 1993, *MNRAS*, 265, 213

Gerhard, O., Jeske, G., Saglia, R. P., & Bender, R. 1998, *MNRAS*, 295, 197

Gerhard, O., Kronawitter, A., Saglia, R. P., & Bender, R. 2001, *AJ*, 121, 1936

Governato, F., Mayer, L., Wadsley, J., Gardner, J. P., Willman, B., Hayashi, E., Quinn, T., Stadel, J., & Lake, G. 2002, *astro-ph/0207044*

Guiderdoni, B. & Rocca-Volmerange, B. 1987, *A&A*, 186, 1

Haehnelt, M. G., Steinmetz, M., & Rauch, M. 1998, *ApJ*, 495, 647

Halliday, C., Davies, R. L., Kuntschner, H., Birkinshaw, M., Bender, R., Saglia, R. P., & Bagley, G. 2001, *MNRAS*, 326, 473

Hernquist, L. 1992, *ApJ*, 400, 460

Hernquist, L. 1993, *ApJ*, 409, 548

Jansen, R. A., Franx, M., Fabricant, D., & Caldwell, N. 2000, *ApJS*, 126, 271

Jedrzejewski, R. & Schechter, P. L. 1988, *ApJ*, 330, L87

Katz, N. 1992, *ApJ*, 391, 502

Katz, N. & White, S. D. M. 1993, *ApJ*, 412, 455

Kennicutt, R. C. 1998, *ARA&A*, 36, 189

Kronawitter, A., Saglia, R. P., Gerhard, O., & Bender, R. 2000, *A&AS*, 144, 53

Mihos, J. C. & Hernquist, L. 1994, *ApJ*, 437, L47

Naab, T. & Burkert, A. 2001, *ApJ*, 555, L91

Navarro, J. F. & Steinmetz, M. 1997, *ApJ*, 478, 13

Navarro, J. F. & Steinmetz, M. 2000, *ApJ*, 538, 477

Navarro, J. F. & White, S. D. M. 1993, *MNRAS*, 265, 271

Navarro, J. F. & White, S. D. M. 1994, *MNRAS*, 267, 401

Nieto, J.-L. & Prugniel, P. 1987, *A&A*, 186, 30

Partridge, R. B. & Peebles, P. J. E. 1967, *ApJ*, 147, 868

Peebles, P. J. E. 2002, in *ASP Conf. Ser.* 283, *A New Era in Cosmology*, ed. N. Metcalfe & T. Shanks (San Francisco: ASP), in press

Peletier, R. F. 1993, *A&A*, 271, 51

Prochaska, J. X. & Wolfe, A. M. 1998, *ApJ*, 507, 113

Prugniel, P., Nieto, J.-L., & Simien, F. 1987, *A&A*, 173, 49

Rix, H., de Zeeuw, P. T., Cretton, N., van der Marel, R. P., & Carollo, C. M. 1997, *ApJ*, 488, 702

Scalo, J. M. 1986, *Fundamentals of Cosmic Physics*, 11, 1

Sommer-Larsen, J., Gotz, M., & Portinari, L. 2002a, *astro-ph/0204366*

Sommer-Larsen, J., Götz, M., & Portinari, L. 2002b, *Ap&SS*, 281, 519

Springel, V. 2000, *MNRAS*, 312, 859

Steinmetz, M. 1996, *MNRAS*, 278, 1005

Steinmetz, M. & Mueller, E. 1994, *A&A*, 281, L97

Steinmetz, M. & Muller, E. 1995, *MNRAS*, 276, 549

Steinmetz, M. & Navarro, J. F. 2002, *New Astronomy*, 7, 155

Surma, P. & Bender, R. 1995, *A&A*, 298, 405

Thomas, D. 2001, *Ap&SS*, 276, 831

Toomre, A. 1977, in *The Evolution of Galaxies and Stellar Populations*, ed. B. Tinsley & R. Larson (New Haven, CN: Yale Univ. Press), 401

van der Marel, R. P. & Franx, M. 1993, *ApJ*, 407, 525